Chemical Physics Letters 754 (2020) 137657

Contents lists available at ScienceDirect

Chemical Physics Letters

journal homepage: www.elsevier.com/locate/cplett

Research paper

Structural and Photo-luminescence examination of red emissive Eu^{3+}-doped nanophosphor synthesized via solution-combustion method

Heena Dahiya[a], Anju Siwach[a], Manju Dahiya[a], Amanvir Singh[a], Sonia Nain[a], Mandeep Dalal[b], S.P. Khatkar[b], V.B. Taxak[b], Dinesh Kumar[a,*]

[a] Department of Chemistry, Deenbandhu Chhotu Ram University of Science & Technology, Murthal, Sonepat 131039, India
[b] Department of Chemistry, Maharshi Dayanand University, Rohtak 124001, India

HIGHLIGHTS

- Eu^{3+} -doped $Ba_3YP_3O_{12}$ nanophosphors have been fabricated via solution-combustion route for the first time.
- Phase and structure morphology of the powder sample was determined by Rietveld analysis using XRD pattern and TEM image.
- The CIE color coordinates confirm intense red emission with high color purity.
- These nanophosphors are appropriate aspirant for solid state lighting.

ARTICLE INFO

Keywords:
Solution-Combustion
Rietveld, Nanocrystal
Optical Properties
No-concentration-quenching

ABSTRACT

Eu^{3+}-doped $Ba_3YP_3O_{12}$ nanoparticles were prepared by the solution-combustion method. Rietveld refinement confirmed that the system crystallizes in cubic structure with I-43d (2 2 0) space group. Spherical shaped particles in nano range were observed which are responsible for improved luminescence. The 4.9 eV optical band-gap of the host shows that it as a good aspirant for lanthanide activators. The Photoluminescence emission spectrum demonstrates prevailing emission peak assigning to $^5D_0 \rightarrow {}^7F_2$ transition at 612 nm of Eu^{3+} ions when energized at a wavelength of 394 nm. CIE color coordinates (x, y) exposed red emission, making this nanophosphor a potential candidate in NUV excited WLEDs.

1. Introduction

Trivalent lanthanide-doped phosphors have gained the attention of the scientists in the discipline of life, chemical, physical and material sciences as a result of their potential applications in plenty of devices, for example, sensors innovation, bio-imaging, optoelectronics, luminescent solar collectors, color display and laser cooling [1–5]. Furthermore, special concern has been given regarding the investigation of White Light Emitting Diodes (WLEDs) owing to the attributes like less energy usage, budget-friendly, environmentally favorable and solid-state-lighting diligence [6–10]. Currently, WLEDs bearing remarkable color temperature and high color rendering index are being produced utilizing a near ultra-violet (NUV) LED coated by red, green and blue phosphors [11–14]. Besides, a unique endeavor has been paid to explore trivalent europium doped red-light emitting nanophosphors due to the sharp spectral bands acquired on account of 4*f* electrons intra-configurational transitions [15,16]. An extensive array of host lattices has been investigated to fabricate prominent nanophosphors. However, no attempt has been made to examine the surface morphology and optical assets of $Ba_3Y_{1-x}Eu_xP_3O_{12}$ nanoparticles. The standard cubic $Ba_3YP_3O_{12}$ has I-43d (2 2 0) space group with lattice parameters a (Å) = 10.4655, $\alpha = \beta = \gamma = 90^\circ$ and unit cell volume equivalent to 1146.25 $Å^3$ [17,18].

Nowadays, a few wet-chemical methods, for example, the sol-gel approach, microwave-assisted synthesis, solution-combustion method, solvothermal method, and hydrothermal technique are broadly employed to fabricate nanoparticles of desirable scale [19,20]. In this case, the solution-combustion technique has been utilized knowing the fact that it is a novel procedure for the synthesis of phosphor with excellent crystallite size and also this method produces a high-quality controlled homogenous product in a less duration of time deprived of employing highly expensive temperature furnaces. The obtained powdered samples are homogenous, single-phased and highly pure [21–24]. To the best of our knowledge, this is the first study to fabricate

* Corresponding author.
E-mail address: dineshdalal8@rediffmail.com (D. Kumar).

https://doi.org/10.1016/j.cplett.2020.137657
Received 17 January 2020; Received in revised form 28 April 2020; Accepted 27 May 2020
Available online 29 May 2020

$Ba_3Y_{1-x}Eu_xP_3O_{12}$ nanophosphor via a urea-based solution-combustion method. In this work, the optoelectronic examination of red-emissive and single-phase $Ba_3Y_{1-x}Eu_xP_3O_{12}$ nanophosphors, as well as their crystal morphology, was explored. We have further examined the impact of trivalent europium ions concentration in $Ba_3YP_3O_{12}$ on the account of crystal structure parameters. The Rietveld refinement of $Ba_3Y_{0.10}Eu_{0.90}P_3O_{12}$ divulged that it solidifies in a cubic lattice with I-43d (2 2 0) space group. The produced excitation and emission spectrum investigated the photoluminescence attributes of the powders recommending their potential application in WLEDs utilizing near ultra-violet LED chip excitation. For the assertion of particle measure in nanoarray and their surface morphology of the synthesized europium doped nanophosphors, we have used the Powder X-ray diffraction (PXRD) and Transmission Electron Microscopy (TEM) techniques to examine $Ba_3Y_{1-x}Eu_xP_3O_{12}$. Furthermore, the results obtained from the TEM micrograph were well justified with the particle size evaluation using the Scherrer's equation. The PL excitation spectra of these nanophosphors demonstrate absorption at 394 nm ascribed to the $^7F_0 \rightarrow {}^5L_6$ transition. Moreover, these phosphor samples find usage in plasma display panels working under NUV and Eu^{3+} doped phosphate-based solid-state laser.

2. Experimental

2.1. Material and synthesis

Lanthanides-doped $Ba_3Y_{1-x}Eu_xP_3O_{12}$ (x = 0.01–1.00) nanocrystals were prepared utilizing the solution-combustion technique. The raw materials required for the fabrication of luminescent material were $Y(NO_3)_2{\cdot}6H_2O$, $Ba(NO_3)_2$, $Eu(NO_3)_3{\cdot}6H_2O$, $(NH_4)_2HPO_4$ and NH_2CONH_2. The raw materials were measured stoichiometrically and mixed in the least volume of triple-distilled water in a beaker. Also, the quantity of urea required was determined by utilizing reducing and oxidizing valencies of the fuel and the oxidizer [25]. In the solution-combustion method, urea served as a fuel and was oxidized using nitrate ions [26–28]. Now, the solution was placed in an oven maintained at 500 °C. In the beginning, the sample solution experiences quick dehydration and effervescing followed with disintegration and releasing of the gases. These gases burn with a fire producing voluminous flaky solid material. The attained material was then cooled and fine-grained. The obtained material was then cooled and pulverized. At last, powders were calcined at 1300 °C for 3 h in a furnace and cooled to room temperature, and the samples were used for different characterizations.

2.2. Materials characterization

A series of synthesized nanophosphors of $Ba_3Y_{1-x}Eu_xP_3O_{12}$, calcined at 1300 °C temperature was portrayed utilizing an Ultima-IV powder X-ray diffractometer (PXRD). The diffraction patterns were measured from 2θ = 20° − 60° with a scanning pace of 2° min^{-1} utilizing Cu Kα radiation (λ = 1.5404 Å) at 40 mA and 40 kV cylinder current and cylinder voltage, respectively. The quantitative and the qualitative phase investigation of the $Ba_3Y_{0.10}Eu_{0.90}P_3O_{12}$ were scrutinized utilizing Rietveld refinement by "FULLPROF" program. The surface morphological attributes were achieved by using a Technai G^b Transmission Electron Microscopy (TEM) instrument. Diffuse Reflectance Spectrum (DRS) was recorded by employing Shimadzu UV-3600 assembled with an integrated sphere. To examine the band-gap energy of the host sample when measured at 200–800 nm wavelength range BaSO4 was used as a standard reference. Photoluminescent excitation (PLE) and photoluminescent emission (PL), lifetime decay curve and color co-ordinates of the $Ba_3Y_{1-x}Eu_xP_3O_{12}$ (x = 0.10–1.00) powder samples in the UV– visible range were examined utilizing a Hitachi F-7000 fluorescence spectrophotometer fitted with Xe-lamp as the excitation source.

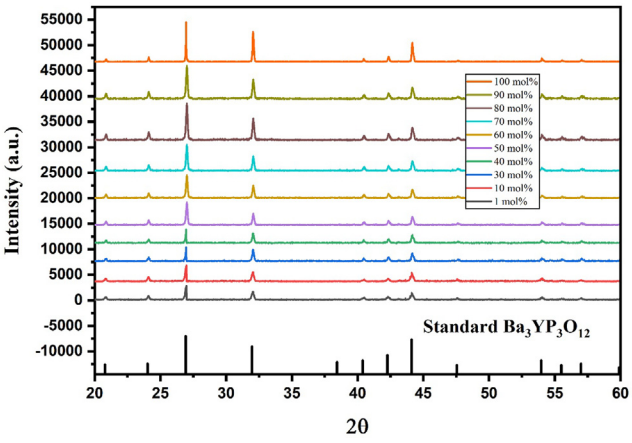

Fig. 1. XRD profile of $Ba_3YP_3O_{12}$:xEu^{3+} (x = 0.01–1.0) nanophosphors alongwith standard data of $Ba_3YP_3O_{12}$.

3. Results and discussion

3.1. Structural analysis

Fig. 1. displays the X-ray diffraction profile of a synthesized series $Ba_3Y_{1-x}Eu_xP_3O_{12}$ (x = 0.10–1.00) nanocrystals calcined at 1300 °C. The outcomes, when compared with the standard JCPDS data, affirm that there are no detectable impurity peaks in the XRD profile patterns even at high doping concentration, representing that the synthesized samples are of single-phase and the trivalent europium ions have entered the $Ba_3YP_3O_{12}$ host effectively without altering the crystal structure prototype. To study the crystal structure and phase information of the nanophosphors, we did the Rietveld refinement utilizing the "FULLPROF" program. Fig. 2. showing that nanophosphor ($Ba_3Y_{0.10}Eu_{0.90}P_3O_{12}$) solidifies into a cubic structure with the I-43d (2 2 0) space group. The refined unit cell parameters were resolved to be a (Å) = 10.5656, α = β = γ = 90°, V = 1179.46 $Å^3$ and Z = 4 along with the final residual factors converged to Rp = 9.5%, Rwp = 11.78% and χ^2 = 3.83. The refined parameters direct that the powder sample is well crystallized, and the attained structure is reliable. In the Rietveld plot (Fig. 2), black dot demonstrates the pattern fitting of the theoretically observed XRD profile while red crosses exhibit experimentally calculated X-ray diffraction profile; the blue line shows the level of deviation from the experimental data to the theoretical one.

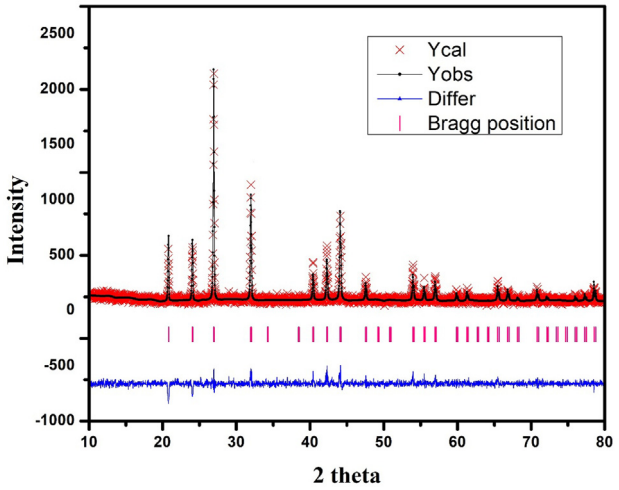

Fig. 2. Rietveld refinement of $Ba_3Y_{0.10}Eu_{0.90}P_3O_{12}$ nanocrystals χ^2 = 3.83, R_{wp} (%) = 11.78, R_p (%) = 9.5.

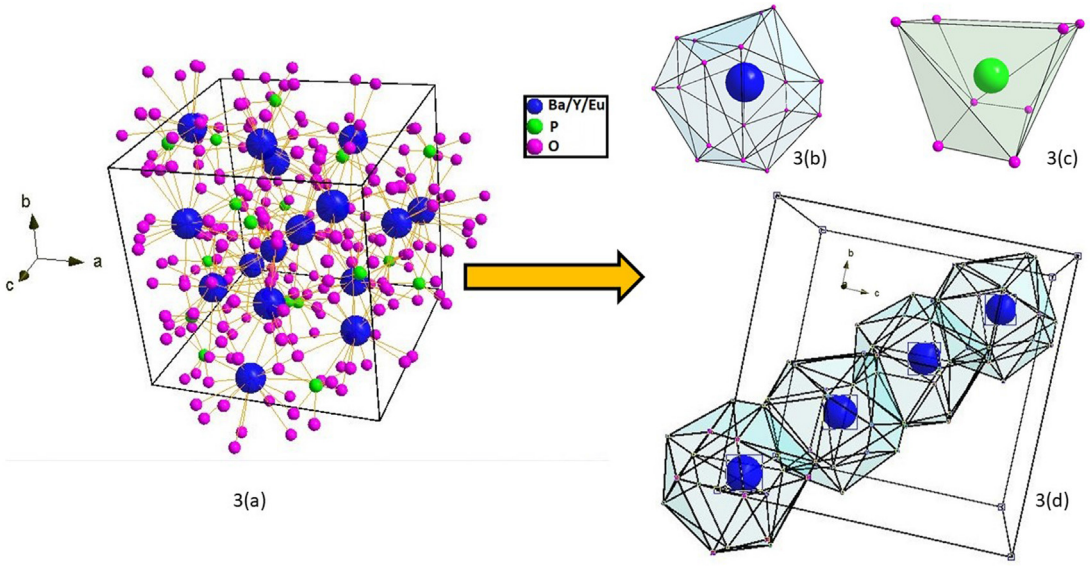

Fig. 3. The typical crystal structure view of $Ba_3Y_{0.10}Eu_{0.90}P_3O_{12}$ (a) the 3-dimensional unit cell, Coordination situation of (b) Ba/Y/Eu atoms and (c) P atom in $Ba_3YP_3O_{12}$ and (d) Partial enlargement structure diagram exhibiting the coordinative environment of few cations occupying Wyckoff positions 16c when viewed through a-axis.

Table 1
Comparison of crystal structure data of $Ba_3Y_{0.10}Eu_{0.90}P_3O_{12}$ nanophosphor with standard $Ba_3YP_3O_{12}$.

Formula	$Ba_3YP_3O_{12}$ (Published)	$Ba_3Y_{0.10}Eu_{0.90}P_3O_{12}$
Formula Weight	785.80	842.545
Symmetry	Cubic	Cubic
Space Group	I −4 3 d (2 2 0)	I −4 3 d (2 2 0)
$a = b = c$ (Å)	10.4655	10.5656
α = β = γ (degree)	90	90
Volume (Å^3)	1146.25	1179.46
Z	4	4
Density (g/cm^3)	4.54	4.74
Pearson Code	tI76	tI76
Wyckoff Sequence	i2h5ba	i2h5ba

Table 2
Refined positions of all atoms and occupancy data for the $Ba_3Y_{0.10}Eu_{0.90}P_3O_{12}$ nanocrystal.

Atom Label	Ion Type	Wyckoff positions	Fill	*x/a*	*y/b*	*z/c*
Ba	Ba^{2+}	16c	0.7450	0.06341 (2)	0.06341 (2)	0.06341 (2)
Y	Y^{3+}	16c	0.0123	0.06341 (2)	0.06341 (2)	0.06341 (2)
Eu	Eu^{3+}	16c	0.2427	0.06341 (2)	0.06341 (2)	0.06341 (2)
P	P^{5+}	12a	1	0.3750	0	0.25
O1	O^{2-}	48e	0.381	0.29570(5)	0.03420(6)	0.11550(8)
O2	O^{2-}	48e	0.719	0.20640(5)	0.06580(5)	0.15620(5)

According to the Rietveld refinement results, there are three autonomous crystallographic atomic sites, including Ba/Y/Eu, 1P and 1O atom. Fig. 3 demonstrates the typical 3d- crystallographic cubic unit structure of the $Ba_3Y_{0.10}Eu_{0.90}P_3O_{12}$ nanophosphor. The blue sphere signifies Ba, Y and Eu atoms sharing the same Wyckoff position at site 16c and adopt an irregular [Ba/Y/EuO_{18}] polyhedrons. Phosphorous (green sphere) are existing in the form of irregular PO_8 units lodging Wyckoff 12a site. Table 1 shows the detailed crystal structural comparison of the host and as-synthesized nanophosphors. In $Ba_3YP_3O_{12}$ crystal structure, Eu^{3+} particles are relied upon to supplant Y^{3+} particles and can be enlightened with the rise in unit cell volume from 1150.36 Å^3 to 1179.46 Å^3 upon doping of $Ba_3YP_3O_{12}$ host matrix with 90 mol% of trivalent europium ion, which can be understood as of bigger ionic radii of Eu^{3+} than Y^{3+} ions. Table 2. displays the Refined positions and occupancy data of all the atoms for $Ba_3Y_{0.10}Eu_{0.90}P_3O_{12}$ nanocrystals. The crystallites size (D) of all the synthesized nanophosphor were appraised employing FWHM (full-width at half-maxima) of the uttermost diffraction peak (3 1 0) by the assistance of Scherrer's equation:

$$D = \frac{0.941\lambda}{(\beta_O^2(2\theta) - \beta_{Si}^2(2\theta))^{\frac{1}{2}} Cos(\theta)} \quad (1)$$

where D implies the average crystallite size, λ is the X-ray wavelength with the value of 0.15406 nm, θ represents the diffraction angle, $\beta_{Si}(2\theta)$ and $\beta_0(2\theta)$ are the FWHM (in radian) of the standard silicon and synthesized sample, respectively [29,30]. The determined mean crystallite magnitude (D) for $Ba_3Y_{0.10}Eu_{0.90}P_3O_{12}$ is 52 nm.

To further examine the morphology and particle size approximation in $Ba_3YP_3O_{12}$: Eu^{3+} sample powder had been inspected by TEM investigation. The Fig. 4. represents the TEM micrograph of the sample $Ba_3Y_{0.10}Eu_{0.90}P_3O_{12}$ calcined at 1300 °C, which demonstrates the small size synthesized crystals with semi-spherical shape and agglomeration

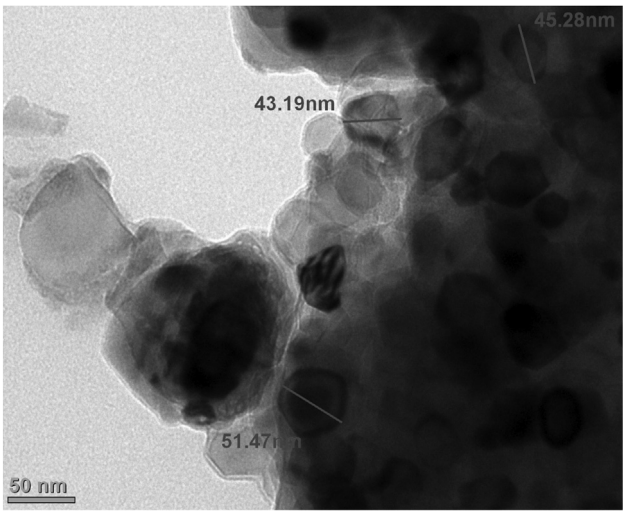

Fig. 4. TEM image of $Ba_3Y_{0.10}Eu_{0.90}P_3O_{12}$ clearly shows the semi-spherical surfaced particles with agglomeration on the scale of 50 nm.

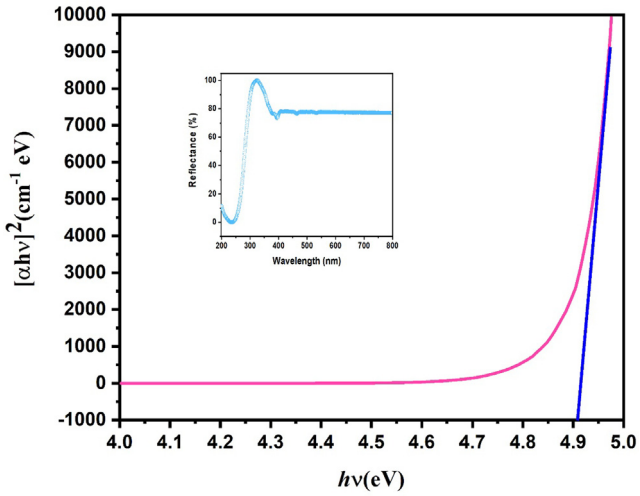

Fig. 5. The relationship between the absorption coefficient and photon energy for $Ba_3YP_3O_{12}$ host matrix and (inset) corresponding diffuse reflectance spectra.

in nano-range. The TEM micrograph evaluation exhibits the typical grain size varying in the range of 35–55 nm, which is in a great concurrence by the value appraised with Scherrer's relation. The obtained nano-scaling array of the synthesized particle plays a vital role in the luminescence proficiency, which might be ascribed to less internal scattering and the high surface is to the volume ratio [31].

Moreover, the optical absorption coefficient of $Ba_3YP_3O_{12}$ and the value of the optical band gap were assessed. The dependable diffuse reflection spectrum is exposed in the inset of Fig. 5 and was utilized in the form of Kubelka-Munk mathematical function to measure the extent of the energy band-gap (E_g). So, the values of band-gap can be estimated by the given below equation [32,33]:

$$[F(R_\infty h\nu]^n = C(h\nu - E_g) \quad (2)$$

where hν signifies the energy of the photon, C represents a proportionality constant, *n* is 0.5, 2, 1.5, 3 implies allowed indirect, allowed direct, forbidden direct and forbidden indirect electronic transitions, respectively and E_g means band gap (eV). Further, the $F(R_\infty)$ (diffuse reflectance) is utilized to appraised the individual absorption value by using the Kubelka-Munk function as [34,35]:

$$F(R_\infty) = \frac{(1 - R_\infty)^2}{2R_\infty} = \frac{K}{S} \quad (3)$$

where K represents the absorption coefficients, S denotes the scattering coefficients, and R_∞ corresponds to the reflection coefficient (relative magnitudes of R_{sample} and $R_{standard}$). The E_g value of $Ba_3YP_3O_{12}$ can be attained by extrapolation of the straight line of $F(R_\infty)$ hν vs hν associated to the energy axis displayed in Fig. 5. Thus, it exposed experimental band-gap energy of 4.92 eV.

3.2. Optical properties

Fig. 6. demonstrates the photoluminescent excitation (PLE) spectra of $Ba_3YP_3O_{12}$: xEu^{3+} (x = 0.20, 0.30, 0.40, 0.50, 0.60, 0.70, 0.80, 0.90 and 1.00) nanophosphors when monitored at λ_{em} = 612 nm ascribed to $^5D_0 \rightarrow {}^7F_2$ emission transition of Eu^{3+} ion in the host matrix. The observed excitation profile divulged indistinguishable spectroscopic spectra, irrespective of change in Eu^{3+} concentration (x), which comprises a few sharp excitation peaks somewhere in the range of 300 to 500 nm. The observed sharp excitation peaks at 319, 361, 381, 394, 414, 465 and 487 nm were attributed to the $^7F_0 \rightarrow {}^5H_6$, $^5D_4$, $^5G_3$, $^5L_6$, $^5D_3$, $^5D_2$ and $^5D_1$ transitions of Eu^{3+}, correspondingly and are intra-configurational $4f-4f$ forbidden transitions which show that the product can be efficaciously excited by near-UV LED chip and has a

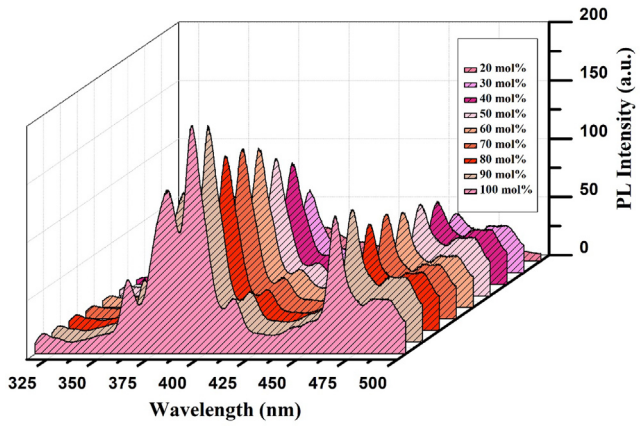

Fig. 6. Excitation spectrum of $Ba_3Y_{1-x}Eu_xP_3O_{12}$ (x = 0.20–1.0) nanophosphor studied at λ_{em} = 612 nm.

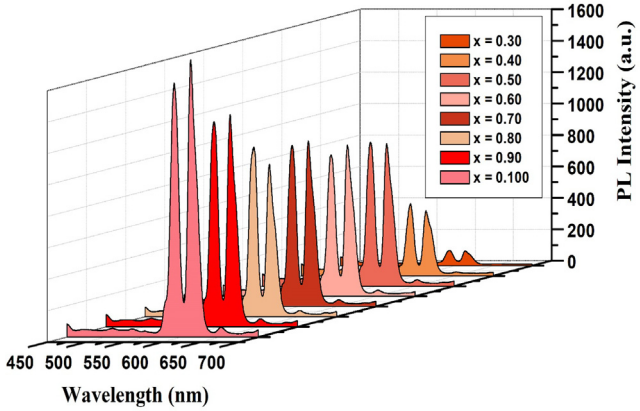

Fig. 7. Emission spectrum of $Ba_3Y_{1-x}Eu_xP_3O_{12}$ (x = 0.30–1.0) nanophosphor monitored at λ_{ex} = 394 nm.

potential for the commercial solid-state LEDs [36,37].

Furthermore, photoluminescence emission (PL) of $Ba_3YP_3O_{12}$: xEu^{3+} (x = 0.30–1.00) nanophosphors were recorded when adjusted at excitation wavelength (λ_{ex}) 394 nm as shown in Fig. 7. The two dominating emission peaks focused at 612 (red light), and 591 nm (orange light) play a significant role in the photoluminescence phenomenon. The $^5D_0 \rightarrow {}^7F_2$ transition belongs to the forced electric-dipole transition. It is hypersensitive to the site symmetry of the activated ions. At the same time, another little less intense emission peak of $^5D_0 \rightarrow {}^7F_1$ transition is ascribed to the magnetic-dipole transition of Eu^{3+} ions, which is found to be insensitive to the crystalline position of the Eu^{3+} ion. Along with two main peaks in the PLE spectra, four weak peaks are observed at 470, 510, 552 and 651 nm and are attributed to $^5D_2 \rightarrow {}^7F_1$, $^5D_1 \rightarrow {}^7F_2$, $^5D_0 \rightarrow {}^7F_0$ and $^5D_0 \rightarrow {}^7F_3$ transitions, respectively [38–40]. The schematic energy level diagram of Eu^{3+} in the $Ba_3YP_3O_{12}$ host matrix is shown in Fig. 8, showing excitation of the electrons at 394 nm to the $^5L_6$ and ^5D_J levels of Eu^{3+} ion. The electrons lying in $^5L_6$ and various levels of ^5D_J first relax non-radiatively to the $^5D_0$ level followed by radiative transitions to ^7F_J (J = 0, 1, 2, and 3) levels of Eu^{3+} ions.

As a series of Eu^{3+}-doped $Ba_3YP_3O_{12}$ nanophosphors were fabricated, and their optimal dopant concentration along with luminescent properties was explored. All the powder samples of the series displayed trademark emissions related to Eu^{3+} with comparable spectroscopic profiles, while their PL intensities varied when Eu^{3+} ions concentration was increased. Fig. 9 displays that PL emission intensities increase dully with increments in the dopant ion concentration from 20 to 100%; hence it predicts the no-concentration quenching.

Furthermore, the room-temperature decay profiles for the samples

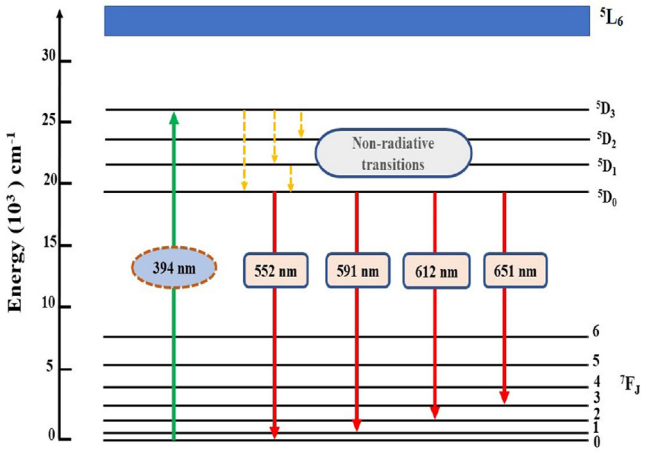

Fig. 8. Schematic Energy level diagram for Eu^{3+} doped $Ba_3YP_3O_{12}$ nanophosphor.

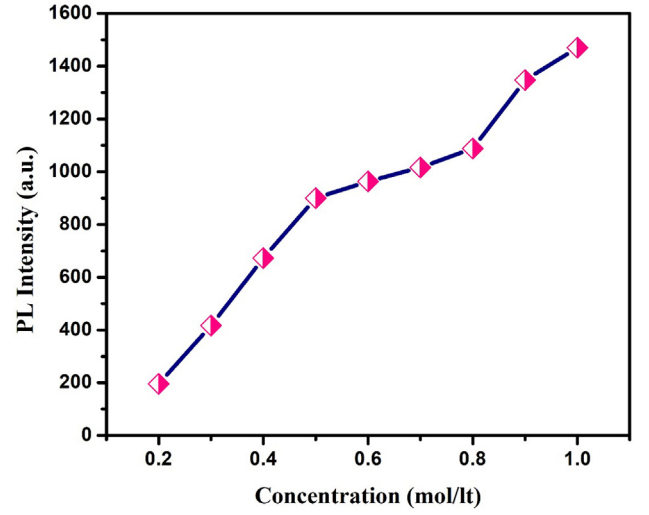

Fig. 9. Graph showing relationship between PL intensity and Eu^{3+} ions concentration in $Ba_3Y_{1-x}Eu_xP_3O_{12}$ (x = 0.20–1.00) host matrix.

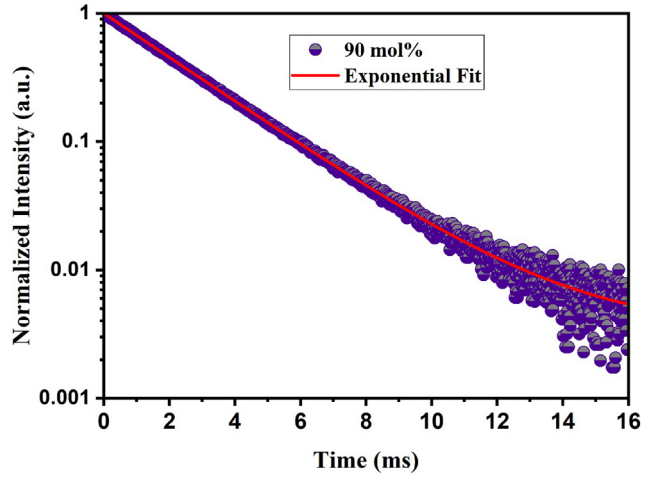

Fig. 10. The luminescence decay curve for 612 nm ($^5D_0 \rightarrow {}^7F_2$ of Eu^{3+}) emission of $Ba_3Y_{0.10}Eu_{0.90}P_3O_{12}$ nanophosphor.

of $Ba_3Y_{1-x}Eu_xP_3O_{12}$ (x = 0.10–1.00) nanophosphors subjected to λ_{ex} = 394 nm were obtained as displayed in Fig. 10. The attained decay data was found to be well-fitted with the double exponential function as [41,42]:

$$I(t) = \left[A_1 \exp\left(-\frac{t}{\tau_1}\right) + A_2 \exp\left(-\frac{t}{\tau_2}\right)\right] \quad (4)$$

where t is the time, A_1 and A_2 are the constants of intensity and τ_1 and τ_2 represent the two different decay times once intensity declines to 1/e of the initial intensity. Based on this data, the average lifetime decay (τ_{avg}) can be appraised by utilizing the following equation:

$$\tau_{avg} = \frac{(A_1\tau_1^2 + A_2\tau_2^2)}{(A_1\tau_1 + A_2\tau_2)} \quad (5)$$

Usually, the double-exponential fit is elucidated on the foundation of two dissimilar chemical surroundings of the dopant ions. But, in these samples, due to the equivalent bonding outlines and (Eu–O) interionic distances, the decay process of these particular nanophosphors can be precise by the surface consequence rising after the nano-scaling of the luminescent samples, as described in earlier research works [43,44]. The phenomenon of fast and slow deactivation can be subjected to the locations of the activator ion in the host. It was found that in the cases where crystallite magnitude of the luminous material dwells in nanoarray, depth aspect dominates. The dopants ions existing on the surface were denoted to fast relaxation (τ_1), while the dopant ions located deeply were accountable for the dilatory relaxation action (τ_2). The subsequent lifetime (τ_{avg}) of $^5D_0$ state is the mean of decay times, i.e. τ_1 and τ_2. The decay times for the whole sequence of $Ba_3YP_3O_{12}$: Eu^{3+} nanophosphors are listed in Table 3.

The CIE (Commission Internationale de l'Eclairage) 1931 chromaticity coordinates (x, y) were evaluated to appraise the emission color of $Ba_3Y_{1-x}Eu_xP_3O_{12}$ (x = 0.10–1.00) nanophosphors. MATLAB software package installed with the CIE color calculator program was used to assess the color coordinates and are shown in Fig. 11. The attained CIE color coordinates for all the fabricated phosphors excited with the 394 nm wavelength lie in the red region offering a range of display and lighting applications. The fundament of the European Broadcasting Union (EBU) and standard of NTSC reveal the color purity of the luminescent material as an essential parameter to assess the possibility of the fabricated nanophosphors for WLEDs and displays.

The color purity of the powder was evaluated by using the below-given relation [45]:

$$Color\ \ purity = \frac{\sqrt{(x - x_i)^2 + (y - y_i)^2}}{\sqrt{(x_d - x_i)^2 + (y_d - y_i)^2}} \quad (7)$$

Where, (x_i, y_i = 0.310, 0.316) are the color coordinate of white illumination, (x_d, y_d = 0.684, 0.315) is the CIE coordinate of the dominant emission wavelength and (*x*, *y*) stands for the CIE

Table 3
Photoluminescence lifetime (ms) of $^5D_0$ states, CIE 1931 chromaticity index and *u′* and *v′* coordinates for $Ba_3Y_{1-x}Eu_xP_3O_{12}$ (*x* = 0.20–1.0) nanophosphors.

Eu^{3+} Concentration (mol %)	Life-Time (ms)	CIE Color coordinates (*x*, *y*)	(*u′*, *v′*)
10	2.35	(0.5403, 0.3230)	(0.373, 0.502)
20	2.21	(0.5473, 0.3402)	(0.366, 0.511)
30	2.13	(0.5503, 0.3313)	(0.375, 0.508)
40	2.07	(0.5691, 0.3390)	(0.384, 0.523)
50	1.97	(0.5979, 0.3397)	(0.407, 0.520)
60	1.88	(0.6932, 0.3394)	(0.488, 0.538)
70	1.74	(0.625, 0.3401)	(0.429, 0.525)
80	1.64	(0.6398, 0.3198)	(0.460, 0.518)
90	1.53	(0.6612, 0.3189)	(0.481, 0.522)
100	1.41	(0.6531, 0.3203)	(0.472, 0.521)

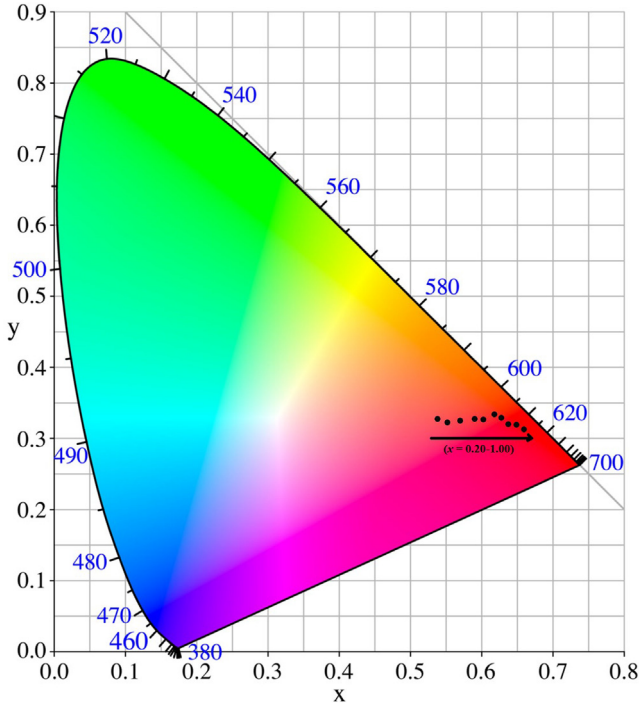

Fig. 11. Chromaticity diagram and coordinates (x,y) according to CIE 1931 for $Ba_3Y_{1-x}Eu_xP_3O_{12}$ (x = 0.20–1.0) nanophosphors.

chromaticity coordinate of the sample. In this present work, $Ba_3Y_{0.10}Eu_{0.90}P_3O_{12}$ powder sample owing the value of (x, y) = (0.6612, 0.3189) exhibits the color purity around 99.29%. Also, according to the latest CIE 1976 standard u′ and v′ coordinates were assessed by utilizing the Eqs. (8) and (9), respectively. Whereas, Fig. 12 displays the chromaticity coordinates in terms of u′ and v′ uniform color space for $Ba_3Y_{0.10}Eu_{0.90}P_3O_{12}$ nanophosphor sample. The appraised data of the CIE co-ordinates (x, y) and u′, v′ co-ordinates values of the luminescent powder samples are presented in Table 3 [46,47].

$$u' = \frac{4x}{-2x + 12y + 3} \tag{8}$$

$$v' = \frac{4y}{-2x + 12y + 3} \tag{9}$$

where $n = \frac{(x - x_e)}{(y - y_e)}$ implies the inverse slope line; x_e = 0.3320, y_e = 0.1858 represents the epicenter; and (x, y) signifies the chromaticity CIE coordinates of the samples. These outcomes exposed that the Eu^{3+}-activated $Ba_3YP_3O_{12}$ nanophosphors owned decent CIE chromaticity coordinate and high color purity, and thus can be considered as a good aspirant in the field of WLEDs as a red-emitting luminescent material.

4. Conclusion

Single-step urea assisted solution-combustion method had been successfully used to fabricate a series of $Ba_3Y_{1-x}Eu_xP_3O_{12}$ (x = 0.10 – 1.00) nanocrystals. The Rietveld refinement scrutiny disclosed that $Ba_3Y_{0.10}Eu_{0.90}P_3O_{12}$ nanophosphor sample formed in single-phase cubic structure with the I-43d (2 2 0) space group and lattice

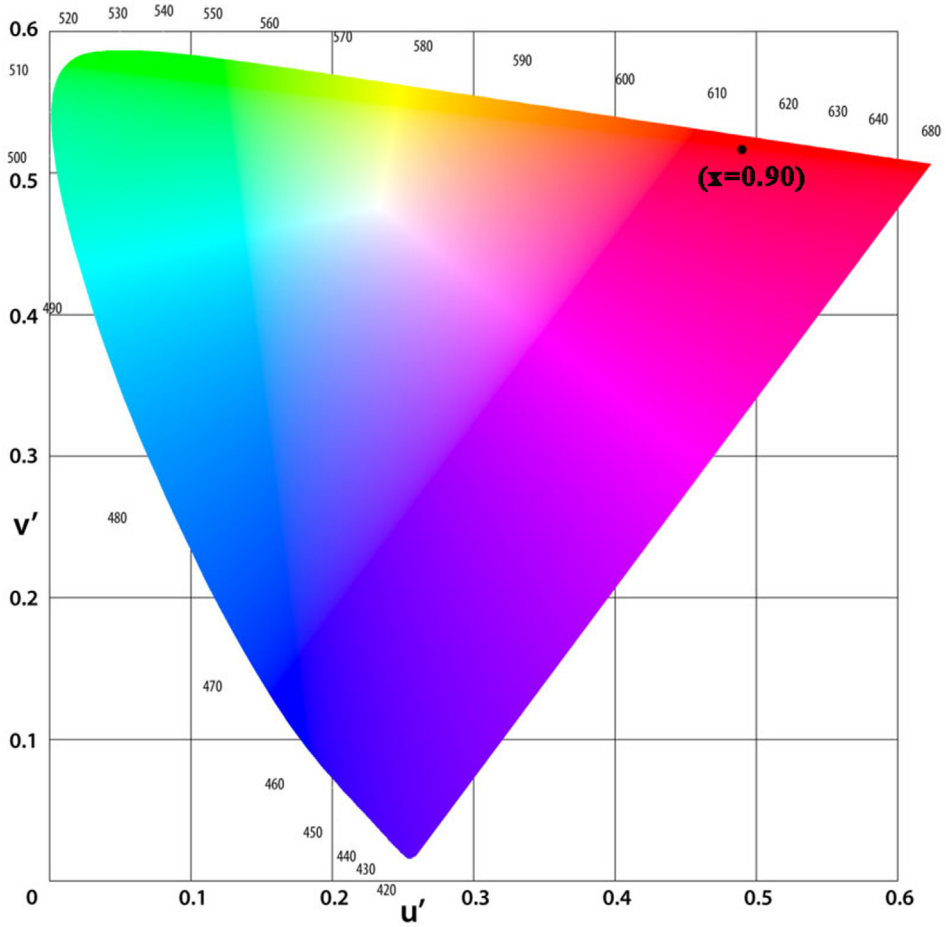

Fig. 12. Chromaticity diagram and coordinates in the terms of u′ and v′ uniform color space according to CIE 1976 for $Ba_3Y_{0.10}Eu_{0.90}P_3O_{12}$ nanophosphor.

parameters were found to be a = b = c = 10.5656 Å, α = β = γ = 90°, V = 1179.46 Å^3 and Z = 4, the refinement parameters are observed to be Rp = 9.5%, Rwp = 11.78% and χ2 = 3.83. Because of the integration of Eu^{3+} ions in the host and integral in the same lattice sites as Y^{3+} ions, the cell volume of the unit increased. Surface morphological investigations revealed semi-spherical shaped particles in the nano range accountable for visible luminescence in the visible region. The Photoluminescence emission spectrum exhibited a prevailing emission peak at 612 nm attributed to $^5D_0 \rightarrow {}^7F_2$ transition of Eu^{3+} ions when monitored at 394 nm wavelength and unveiled as a noteworthy red component for WLEDs. The Photoluminescence spectrum shows that there is no-concentration quenching in the Eu^{3+}-doped $Ba_3YP_3O_{12}$ red-emitting nanophosphors. So, the results of CIE color coordinates (*x*, *y*) imitated red emission, making this nanophosphor an effective applicant in NUV excited WLEDs.

Declaration of Competing Interest

The authors declare that they have no known competing financial interests or personal relationships that could have appeared to influence the work reported in this paper.

Acknowledgement

One of the authors, Heena Dahiya sincerely acknowledge The Haryana State Council for Science and Technology as HSCST Fellowships (HSCST Award No.: HSCST/1797) for the financial support.

References

[1] S. Chahar, R. Devi, M. Dalal, P. Boora, V.B. Taxak, S.P. Khatkar, Structural and photoluminescent analysis in Judd-Ofelt framework of color tunable $SrGd_{2(1-x)}Eu_{2x}Al_2O_7$ nanophosphor for white light emitting materials, J. Lumin. 194 (2018) 271–278.
[2] M. Tian, P. Li, Z. Wang, X. Teng, Z. Li, J. Cheng, Y. Sun, C. Wang, Z. Yang, Synthesis, color-tunable emission, thermal stability, luminescence and energy transfer of Sm^{3+} and Eu^{3+} single-doped $M_3Tb(BO_3)_3$ (M = Sr and Ba) phosphors, Cryst. Eng. Comm. 18 (2016) 6934–6947.
[3] L. Zhou, J. Huang, F. Gong, Y. Lan, Z. Tong, J. Sun, A new red phosphor $LaNb_{0.7}0_{V0.3}0_O4$: $^{Eu}3+$ for white light-emitting diodes, J. Alloys Compd. 495 (2010) 268–271.
[4] J.T. Ingle, R.P. Sonekar, S.K. Omanwar, Y. Wang, L. Zhao, Combustion synthesis and photoluminescence study of novel red phosphor (Y_{1-x-y}, Gd_x)BaB_9O_{16}:$Eu^{3+}{}_y$ for display and lighting, J. Alloys Compd. 608 (2014) 235–240.
[5] A.A. Ansari, A.K. Aldalbahi, J.P. Labis, M.A. Manthrammel, Impact of surface coating on physical properties of europium-doped gadolinium fluoride microspheres, J. Fluor. Chem. 199 (2017) 7–13.
[6] X. Wang, Z. Zhao, Q. Wu, Y. Li, C. Wang, A. Mao, Y. Wang, Synthesis, structure, and luminescence properties of $SrSiAl_2O_3N_2$:Eu^{2+} phosphors for light-emitting devices and field emission displays, Dalton Trans. 44 (2015) 11057–11066.
[7] J. Feng, Q. Wang, P. Li, L. Ye, J. Xiang, G. Peng, Y. Du, M. Zhu, X. Yuan, Controllable synthesis of ultra-long YCe_xO_y:Eu^{3+} nanowire arrays and fluorescence activation of Ce^{3+}, Mater. Res. Bull. 104 (2018) 44–47.
[8] S. Ponkumar, K. Janaki, D.P. Babu, M.M. Kumar, M.M. Reddy, Flux influenced morphology tailoring and emission color tuning to pure white in ZrO_2:Eu^{3+}phosphors, J. Lumin. 201 (2018) 345–349.
[9] S. Ye, F. Xiao, Y.X. Pan, Y.Y. Ma, Q.Y. Zhang, Phosphors in phosphor-converted white light-emitting diodes: Recent advances in materials, techniques and properties, Mater. Sci. Eng. R. 71 (2010) 1–34.
[10] A.A. Ansari, M.A. Siddiqui, A. Khan, N. Ahmad, M. Alam, A.M.E. Toni, A.A.A. Khedairy, Luminescent surface-functionalized mesoporous core-shell nanospheres and their cytotoxicity evaluation, Colloids Surf. A Physicochem. Eng. Asp. 573 (2019) 146–156.
[11] H. Zhu, X. Liu, R. Fu, Y. Shi, H. Wang, Q. He, X. Son, Luminous efficiency enhancement of WLEDs via patterned RGB phosphor arrays, J. Lumin. 211 (2019) 1–7.
[12] Z. Chen, J.H. Zhang, S. Chen, M.Y. Lin, C.Q. He, G.D. Xu, M.M. Wang, X.F. Yu, J.Q. Zou, K. Guo, Preparation and luminescence property of Eu^{2+}, Mn^{2+} co-doped silicates phosphors for white LED, J. Alloy. Compd. 632 (2015) 756–759.
[13] S. Al-Waisawy, A.F. George, W.M. Jadwisienczak, F. Rahman, Preparation of balanced trichromatic white phosphors for solid-state white lighting, Luminescence 32 (2017) 791–799.
[14] A.A. Ansari, Mesoporous luminescent GdF3: Tb@LaF3@SiO2 nanorods: comparative structural and optoelectronic studies, J. Porous Mater. 26 (2019) 335–342.
[15] Y. Wang, J. Tang, X. Huang, L. Jiang, Luminescence properties of Eu^{3+}:NaGd$(WO_4)_2$ nanoparticles and nanorods, J. Rare Earth. 34 (2016) 118–124.
[16] T. Wang, Y. Hu, L. Chen, X. Wang, M. He, An intense red-emitting phosphor $Sr_3Lu(PO_4)_3$:Eu^{3+} for near ultraviolet light emitting diodes application, Ceram Int. 42 (2016) 3659–3665.
[17] Z. Yang, P. Liu, J. Li, Q. Yang, L. Lv, Y. Zhao, A novel yellow luminescent material $Ba_3Y(PO_4)$ 3: $^{Eu}2+$, J. Alloy. Compd. 578 (2013) 118–120.
[18] F. Yang, Y. Liu, X. Tian, G. Dong, Q. Yu, Luminescence properties of phosphate phosphor $Ba_3Y(PO_4)_3$:Sm^{3+}, J. Solid State Chem. 225 (2015) 19–23.
[19] A. Jain, G.A. Hirata, Photoluminescence, size and morphology of red-emitting Gd_2O_3:Eu^{3+} nanophosphor synthesized by various methods, Ceram. Int. 42 (2016) 6428–6435.
[20] E. Bonturim, L.G. Merízio, R. Reis, H.F. Brito, L.C.V. Rodrigues, M.C.F.C. Felinto, Persistent luminescence of inorganic nanophosphors prepared by wet-chemical synthesis, J. Alloy. Compd. 732 (2018) 705–715.
[21] Y.S. Vidya, K.S. Anantharaju, H. Nagabhushana, S.C. Sharma, H.P. Nagaswarupa, S.C. Prashantha, C. Shivakumara, Combustion synthesized tetragonal ZrO_2: Eu^{3+} nanophosphors: Structural and photoluminescence studies, Spectrochim. Acta Part A: Mol. Biomol. Spectrosc. 135 (2015) 241–251.
[22] K.C. Patil, M.S. Hegde, T. Rattan, S.T. Aruna, Chemistry of Combustion Synthesis, Properties and Applications Nanocrystalline Oxide Materials, World Scientific Publishing Co, Pvt. Ltd., Singapore, 2008.
[23] M. Dalal, V.B. Taxak, S. Lohra, D. Sangwan, S.P. Khatkar, Photoluminescence and structural properties of Eu^{3+} doped $SrZnV_2O_7$ nanocrystals, J. Lumin. 161 (2015) 63–70.
[24] M. Dalal, V.B. Taxak, Sheetal, D. Kumar, S.P. Khatkar, Synthesis and luminescent properties of Tb^{3+} doped $BaLa_2ZnO_5$ nanoparticles, Mater. Chem. Phys. xxx (2014) 1–8.
[25] S. Ekambaram, K.C. Patil, Synthesis and properties of Eu^{2+} activated blue phosphors, J. Alloys Comp. 448 (1997) 7.
[26] C. Zhu, C. Han, T. Akiyama, Controlled synthesis of $LiNi_{0.5}Mn_{1.5}O_4$ cathode materials with superior electrochemical performance through urea-based solution combustion synthesis, RSC Adv. 5 (2015) 49831–49837.
[27] P. Chen, M. Qin, Z. Chen, B. Jia, X. Qu, Solution combustion synthesis of nanosized WOx: characterization, mechanism and excellent photocatalytic properties, RSC Adv. 6 (2016) 83101–83109.
[28] D. Ozer, Z. Ertekin, K. Pekmez, N.A. Oztas, Fuel effects on $Li_2CuP_2O_7$ synthesized by solution combustion method for lithium-ion batteries, Ceram. Int. 45 (2019) 4626–4630.
[29] M.R. Monshi, Foroughi, Modified Scherrer Equation to Estimate More Accurately Nano-Crystallite Size Using XRD, World J. Nano Sci. Eng. 2 (2012) 154–160.
[30] G.K. Williamson, R.E. Smallman, Dislocation densities in some annealed and cold-worked metals from measurements on the X-ray debye-scherrer spectrum, III. Philos. Mag. 1 (1956) 34–46.
[31] A.A. Ansari, N. Ahmad, J.P. Labis, A.M.E. Toni, A. Khan, Aqueous dispersible green luminescent yttrium oxide: terbium microspheres with nanosilica shell coating, Spectrochim. Acta A. 211 (2019) 348–355.
[32] R. Mahajan, S. Kumar, R. Prakash, V. Kumar, R.J. Choudhary, D.M. Phase, X-ray photoemission and spectral investigations of Dy^{3+} activated magnesium pyrophosphate phosphors, J. Alloy. Compd. 777 (2019) 562–571.
[33] H. Guo, Y. Wang, G. Li, J. Liu, P. Feng, D. Liu, Cyan emissive super-persistent luminescence and thermoluminescence in $BaZrSi_3O_9$:Eu^{2+}, P^{r3}+ phosphors, J. Mater. Chem. C 5 (2017) 2844–2851.
[34] R. Naik, S.C. Prashantha, H. Nagabhushana, S.C. Sharma, H.P. Nagaswarupa, K.M. Girish, Effect of fuel on auto ignition route, photoluminescence and photometric studies of tunable red emitting Mg_2SiO_4:Cr^{3+} nanophosphors for solid state lighting applications, J. Alloy. Compd. 682 (2016) 815–824.
[35] Y. Kumar, M. Pal, M. Herrera, X. Mathew, Effect of Eu ion incorporation on the emission behavior of Y_2O_3 nanophosphors: A detailed study of structural and optical properties, Opt. Mater. 60 (2016) 159–168.
[36] A.A. Ansari, A. Khan, J.P. Labis, M. Alam, M.A. Manthrammel, M. Ahamed, M.J. Akhtar, A. Aldalbahi, H. Ghaithan, Mesoporous multi-silica layer-coated Y_2O_3: Eu core-shell nanoparticles: Synthesis, luminescent properties and cytotoxicity evaluation, Mater. Sci. Eng. C 96 (2019) 365–373.
[37] A.A. Ansari, Photochemical studies of monodispersed YPO_4: Eu microspheres: The role of surface modification on structural and luminescence properties, J. Photoch. Photobio. A 343 (2017) 126–132.
[38] J. Shivakumar, R.H. Chikkahanumantharayappa, S. Krishna, G. Nagaraju Ashoka, $CdSiO_3$:Eu^{3+} nanophosphor: one pot synthesis and enhancement of orange–red emission through Li^+ co-doping, J. Mater. Sci.: Mater. Electron. 29 (2018) 12986–12992.
[39] Y. Chu, Q. Zhang, Y. Li, Z. Liu, J. Xu, H. Zeng, H. Wang, Hydrothermal synthesis of $Bi_4Ge_3O_{12}$: Eu^{3+} phosphors with high thermal stability and enhanced photoluminescence property, J. Alloys Compd. 693 (2017) 308–314.
[40] A.A. Ansari, A. Aldalbahi, J.P. Labis, A.M.E. Toni, M. Ahamed, M.A. Manthrammel, Highly biocompatible, monodispersed and mesoporous $La(OH)_3$:Eu@mSiO_2 core-shell nanospheres: Synthesis and luminescent properties, Colloids Surf. B Biointerfaces 163 (2018) 133–139.
[41] X. Xie, J. Chen, Y. Sheng, Y. Song, X. Zhou, X. Zhang, Z. Shi, H. Zou, K. Zheng, Synthesis, structure and multicolor-tunable luminescence of the dandelion-like SiO_2:Ln^{3+} (Ln = Eu, Tb) nanophosphors, New J. Chem. 41 (2017) 5688–5695.
[42] P. Jena, S.K. Gupta, N.K. Verma, A.K. Singh, R.M. Kadam, Energy transfer dynamics and time resolved photoluminescence in $BaWO_4$:Eu^{3+} nanophosphors synthesized by mechanical activation, New J. Chem. 41 (2017) 8947–8958.
[43] L. Li, Z. Leng, W. Zi, S. Gan, Hydrothermal Synthesis of $SrMoO_4$:Eu^{3+}, Sm^{3+} Phosphors and Their Enhanced Luminescent Properties Through Energy Transfer, J. Electron. Mater. 43 (2014) 2588–2596.
[44] H. Suo, C. Guo, T. Li, Broad-Scope Thermometry Based on Dual-Color Modulation

up-Conversion Phosphor $Ba_5Gd_8Zn_4O_{21}:Er^{3+}/Yb^{3+}$, J. Phys. Chem. C 120 (2016) 2914–2924.

[45] S. Som, S. Das, S. Dutta, H.G. Visser, M.K. Pandey, P. Kumar, R.K. Dubey, S.K. Sharma, Synthesis of strong red emitting $Y_2O_3:Eu^{3+}$ phosphor by potential chemical routes: comparative investigations on the structural evolutions, photometric properties and Judd-Ofelt analysis, RSC Adv. 5 (2015) 70887–70898.

[46] L.M. Chepyga, A. Osvet, C.J. Brabec, M. Batentschuk, High-temperature thermographic phosphor mixture YAP/YAG:Dy^{3+} and its photoluminescence properties, J. Lumin. 188 (2017) 582–588.

[47] B.V. Rao, K. Jang, H.S. Lee, S. Yi, J. Jeong, Synthesis and photoluminescence characterization of RE^{3+} ($=Eu^{3+}$, Dy^{3+})-activated $Ca_3La(VO_4)_3$ phosphors for white light-emitting diodes, J. Alloy. Compd. 496 (2010) 251–255.